CHAPTER
THREE

Open-circuit voltage of bulk heterojunction solar cells

Summary

In this chapter, two models for the open-circuit voltage are introduced: First, a model formulated for *p-n* junctions is examined. By studying the dependency of the open-circuit voltage on light intensity, it is concluded that this model does not correctly describe the open-circuit voltage of BHJ solar cells. Whereas the experimental data show a slope S of V_{oc} as a function of $\ln(I)$ is equal to V_t, the *p-n* junction model predicts a slope of nV_t, where n ranges from 1.35 to 1.98. This phenomenon is observed for two different PPV derivatives as donor material. The main cause of this discrepancy lies in the fact that the strong voltage dependence of the photocurrent is not taken into account.

Within the framework of the MIM model an alternative explanation for the open-circuit voltage is presented. Based on the notion that the quasi-Fermi potentials are constant throughout the device, a formula for V_{oc} is derived that consistently describes the open-circuit voltage. Not only is the light intensity dependence predicted by the expression in accordance with the experimental data, but the numerical value of V_{oc} is also correct. Next, the predictions of the MIM model and its relation to other types of solar cells are discussed.

3.1 Open-circuit voltage in *p-n* junction based models

One of the key parameters of photovoltaic devices is the open-circuit voltage, which is the voltage for which the current in the external circuit equals zero. In polymer/fullerene cells limitations of the open-circuit voltage have been attributed to Fermi level pinning[1] and to band bending at the contact due to the injection of charges.[2] For further optimization of solar cell performance fundamental understanding of the mechanisms governing the photovoltaic performance is indispensable.

For a conventional inorganic *p-n* junction solar cell the dark current is given by[3]

$$J_D = J_s\left(e^{\frac{V_a}{nV_t}} - 1\right), \tag{3.1}$$

where J_s is the (reverse bias) saturation current density and n is the ideality factor. The current density under illumination (J_L) is subsequently described by

$$J_L = J_s\left(e^{\frac{V_a}{nV_t}} - 1\right) - J_{\mathrm{ph}}, \tag{3.2}$$

where J_{ph} is the photogenerated current density. For an ideal solar cell it is assumed that the photogenerated current density J_{ph} is voltage-independent, meaning that $J_{\mathrm{ph}} = J_{\mathrm{sc}}$ at any applied voltage. Under this assumption, Eq. (3.2) directly provides an expression for V_{oc}, given by

$$V_{\mathrm{oc}} = nV_t \ln(J_{\mathrm{sc}}/J_s + 1). \tag{3.3}$$

This expression for V_{oc}, derived for conventional inorganic solar cells, has also been used to analyze the temperature dependence of V_{oc} of polymer/fullerene BHJ solar cells.[4,5] Both J_{sc} and J_s depend on temperature, while J_s is not directly measurable. This makes the verification of Eq. (3.3) — and the *p-n* junction model — complicated. A more direct way of testing Eq. (3.3), and consequently Eq. (3.2), is to investigate the dependence of V_{oc} on light intensity since then only J_{sc} changes. Since it has been demonstrated that J_{sc} is nearly linearly dependent on light intensity,[6,7] it follows from Eq. (3.3) that V_{oc} should exhibit a slope of nV_t, when plotted as a function of the logarithm of light intensity. Figure 3.1 confirms that J_{sc} is indeed linear in light intensity for the devices discussed here.

Figure 3.2 shows the current density in dark J_D as a function of applied voltage V_a for MDMO-PPV/PCBM and BEH-PPV/PCBM based solar cells at different temperatures. By fitting the exponential part of the current-voltage characteristics to Eq. (3.1) the ideality factors are determined. The results are summarized in Table 3.1. At room temperature the ideality factor n typically amounts to 1.4 and then increases further with decreasing temperature to 2.0 for MDMO-PPV/PCBM devices and 1.5 for BEH-PPV/PCBM devices at 210 K.

The current voltage characteristic ($J_L - V_a$) of an illuminated (800 W/m^2) MDMO-PPV/PCBM device at room temperature is shown in Fig. 3.3(a), together with the current predicted by Eq. (3.2). It is clear that there is a large discrepancy between the predictions of the model and the experimental data: around zero bias the predicted current is

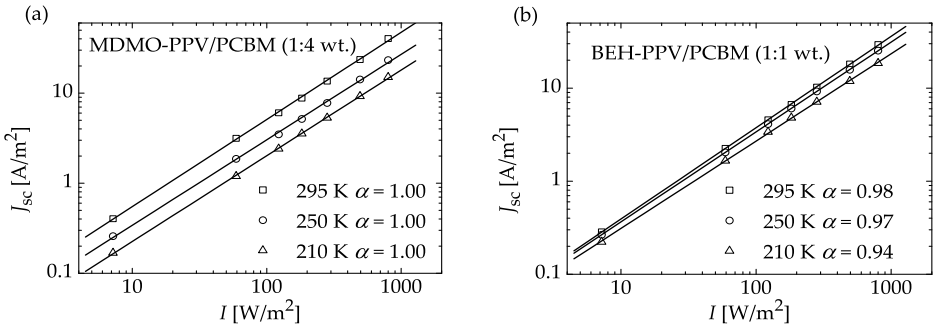

Figure 3.1: The short-circuit current density (symbols) as a function of light intensity for various temperatures, the lines denote fits to $J_{sc} \propto I^{\alpha}$. Part (a) shows data on an MDMO-PPV/PCBM (1:4 wt.) device, while part (b) presents data on a BEH-PPV/PCBM (1:1 wt.) solar cell.

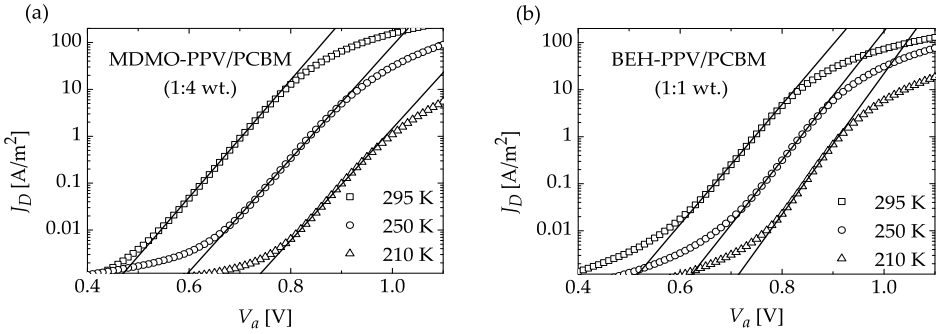

Figure 3.2: Experimental dark current of MDMO-PPV/PCBM (symbols) and fit to the exponential part (lines) at various temperatures. Part (a) shows data on an MDMO-PPV/PCBM (1:4 wt.) device, while part (b) presents data on a BEH-PPV/PCBM (1:1 wt.) solar cell.

Table 3.1: Overview of ideality factors n obtained from Fig. 3.2 and slopes S obtained from Fig. 3.4, for two different photovoltaic devices.

		295 K	250 K	210 K
MDMO-PPV	n	1.34	1.62	1.98
	S [V_t]	1.03	1.01	0.90
BEH-PPV	n	1.35	1.47	1.65
	S [V_t]	1.04	1.01	1.00

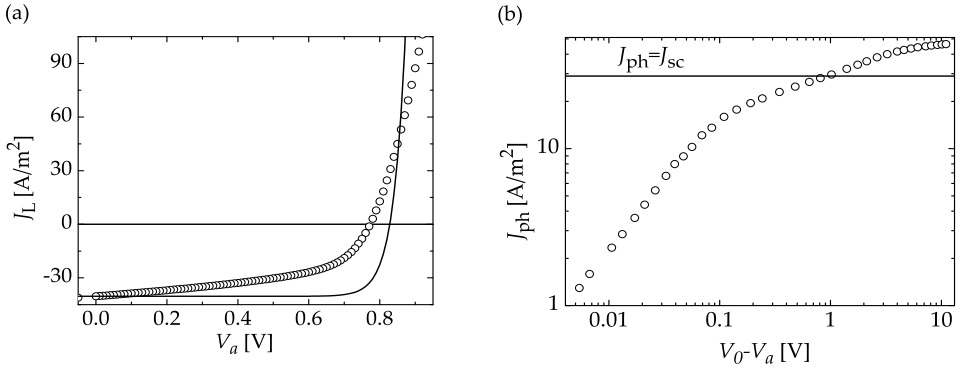

Figure 3.3: (a) Experimental current density under illumination of an MDMO-PPV/PCBM device at 295 K (symbols) and the current density predicted by Eq. (3.2) (line) with n = 1.34 (see Table 3.1). (b) The photocurrent density J_{ph} of an MDMO-PPV/PCBM device (symbols) as a function $V_0 - V_a$. The line denotes the short circuit current density corresponding to the assumption of J_{ph} being constant.

basically constant, in contrast to the experimental current, while near V_{oc} the predicted current is much too high. These observations already strongly indicate that the *p-n* junction model is not applicable to polymer/fullerene bulk heterojunction devices. Fig. 3.4 shows V_{oc} as a function of the logarithm of light intensity at various temperatures for both devices. The experimental data are fitted with a linear function with slope S which is given in Table 3.1 in units of V_t. Surprisingly, the experimental slopes are within experimental error equal to V_t instead of nV_t [Eq. (3.3)] for both devices and all temperatures. Thus, next to the photocurrent (Fig. 3.3) also the light intensity dependence of V_{oc} is not in agreement with the *p-n* junction model.

The main reason for this disagreement is that Eq. (3.3) is based on the assumption of a voltage independent photocurrent density J_{ph}. Recently, it has been shown by Mihailetchi et al.[8] that the photogenerated current shows a very different behavior (see subsection 2.4.2): In Fig. 3.3(b) the photocurrent of an MDMO-PPV/PCBM device is plotted as a function of effective applied voltage, $V_0 - V_a$. Near the compensation voltage, a linear dependence of the photogenerated current upon applied voltage is observed, followed by saturation at high fields. This behavior is caused by the opposite effect of drift and diffusion of charge carriers. Consequently, the assumption of a constant photocurrent is not valid. When the photocurrent near the open-circuit voltage is equated to J_{sc} (solid line) it is clear from Fig. 3.3(b) that the photocurrent is strongly overestimated, hence Eqs. (3.2) and (3.3) cannot be expected to reproduce the experimental data. The fit of Eq. (3.2) to experimental photocurrent data is often improved by including series and shunt resistances.[9] However, the physical meaning of these quantities is not clear.

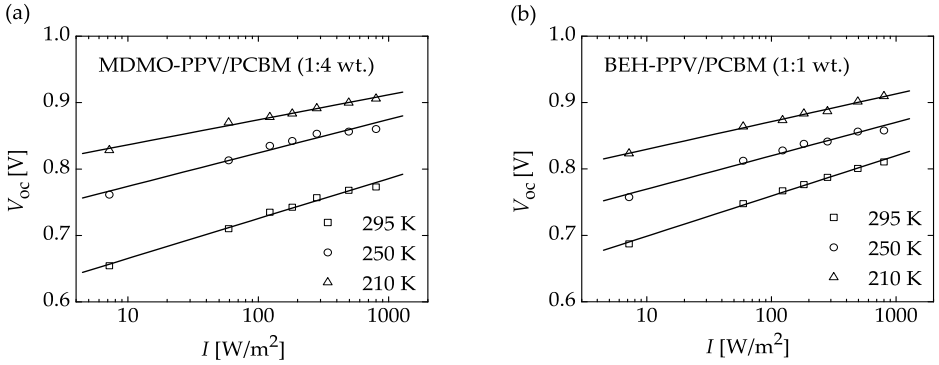

Figure 3.4: V_{oc} as a function of light intensity. The lines denote the linear fits to the experimental data. Part (a) shows data on an MDMO-PPV/PCBM (1:4 wt.) device, while part (b) presents data on a BEH-PPV/PCBM (1:1 wt.) solar cell.

3.2 Open-circuit voltage in the metal-insulator-metal model

3.2.1 General considerations

Which factors govern the open-circuit voltage in the MIM model? Consider the situation as depicted in Fig. 3.5: Due to the fast charge transfer process after exciton formation and subsequent energetic relaxation, the maximum potential that a BHJ solar cell can sustain is limited to the difference between the LUMO level of the donor and the HOMO level of the acceptor, viz.,

$$V_{oc} \leq E_{gap}^{eff}/q. \tag{3.4}$$

Clearly, this even holds for electrodes with a difference in work function $\Phi_{m1,2}$ larger than E_{gap}^{eff}. In practice, however, V_{oc} is significantly smaller than this upper limit. The highest value for V_{oc} is found when Ohmic contacts are used, i.e., $\Phi_{m1} \leq \mathrm{LUMO}(A)$ and $\Phi_{m2} \geq \mathrm{HOMO}(D)$. As these contacts cause high carrier densities in the semiconductor, at least in the vicinity of the electrodes, V_{oc} is typically 0.4 V less than E_{gap}^{eff}/q.[10] In the next subsection the V_{oc} in the case of Ohmic contacts will be extensively studied.

3.2.2 Formula for the open-circuit voltage

Would it be possible to derive a formula for V_{oc} based on the MIM model, as an alternative for Eq. (3.3)? In this subsection, we shall see that this is indeed possible and that the resulting expression does explain the intensity dependence of V_{oc} .

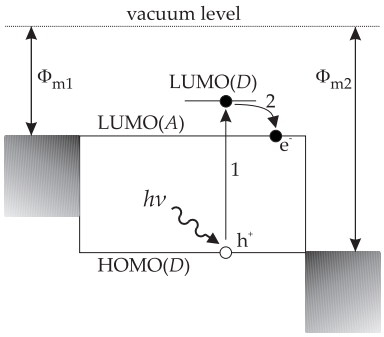

Figure 3.5: Band diagram of a BHJ device sandwiched between two electrodes with work functions $\Phi_{m1,2}$. After photogeneration (1) and electron transfer to the acceptor phase (2), the electron rapidly thermalizes.

As a first step, the quasi-Fermi potentials $\phi_{n,p}$ are introduced as[11]

$$n(p) = n_{\text{int}} \exp\left[(-)\frac{\psi - \phi_{n(p)}}{V_t}\right]. \tag{3.5}$$

The quasi-Fermi potentials are a measure of the deviation from equilibrium of the system. In equilibrium $np = n_{\text{int}}^2$, however,

$$np = n_{\text{int}}^2 \exp\left(\frac{\phi_p - \phi_n}{V_t}\right), \tag{3.6}$$

when the system is not in equilibrium.* The current densities, given in Eq. (2.3), can be rewritten in terms of the quasi-Fermi potentials as

$$J_{n(p)} \propto n(p)\frac{\partial}{\partial x}\phi_{n(p)}. \tag{3.7}$$

As we have seen in chapter 2 (see Fig. 2.12), at open-circuit the current densities are (virtually) zero, consequently, the quasi-Fermi potentials are constant (see Fig. 3.6). Since it is assumed that at the contacts the metal electrodes are in thermal equilibrium with the semiconductor blend, the quasi-Fermi potentials have to be equal to the potential at the contacts. This implies that the difference $\phi_p - \phi_n$ is constant throughout the device and equal to the applied voltage at open-circuit, therefore

$$np = n_{\text{int}}^2 \exp\left(V_{\text{oc}}/V_t\right). \tag{3.8}$$

*Although the definition of $\phi_{n,p}$ in Eq. (3.5) is inspired by the Boltzmann equation, this definition is not limited to circumstances that justify the use Boltzmann's equation, however, Eq.(3.7) is.

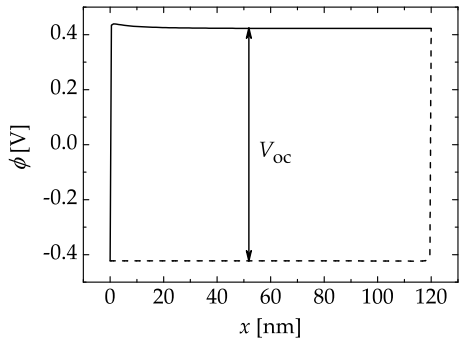

Figure 3.6: The quasi-Fermi potentials $\phi_{n,p}$ for electrons (dashed line) and holes (solid lines) under open-circuit conditions. These values correspond to the fit of an MDMO-PPV/PCBM device as discussed in subsection 2.4.2.

The continuity equation for electrons is given by Eq. (2.20), i.e.,

$$\frac{1}{q}\frac{\partial}{\partial x}J_n(x) = PG_{\mathrm{e-h}} - (1-P)R. \tag{3.9}$$

To a very good approximation, the recombination rate R, given by Eq. (2.12), can be written as $R = k_r np$. Since the current densities are zero, so are their derivatives and hence recombination and generation cancel everywhere in the device. Hence from Eq. (2.20) it follows that

$$G_{\mathrm{e-h}} = k_r np\frac{1-P}{P}. \tag{3.10}$$

Therefore, using Eq. (3.8) and solving for V_{oc}, one has*

$$V_{\mathrm{oc}} = \frac{E_{\mathrm{gap}}^{\mathrm{eff}}}{q} - V_t \ln\left[\frac{(1-P)k_r N_{\mathrm{cv}}^2}{PG_{\mathrm{e-h}}}\right]. \tag{3.11}$$

A similar formula was derived for amorphous silicon *p-i-n* junction solar cells.[12]

What does this equation tell us? Since the dissociation probability P depends on voltage, this is not a strictly explicit relation. However, P only shows a relatively small variation in the voltage range of interest here. Therefore, this equation gives insight into how parameters such as the generation rate (and hence light intensity) affect the open-circuit voltage. Moreover, this formula predicts the right slope S of V_{oc} versus light intensity,

*One might wonder what happens when n and p have their maximum value N_{cv}. In this case, Eq. (3.10) reduces to $PG_{\mathrm{e-h}} = (1-P)k_r N_{\mathrm{cv}}^2$ and hence the argument of the logarithm in Eq. (3.11) is equal to unity, thereby ensuring that $V_{\mathrm{oc}} \leq E_{\mathrm{gap}}^{\mathrm{eff}}/q$, which also follows from Eq. (3.8).

viz., V_t. Furthermore, Eq. (3.11) is consistent with the notion of a field-dependent photocurrent, in contrast to Eq. (3.3), since both drift and diffusion of charge carriers have been taken into account through the use of Eq. (3.7). Equation (3.11) shows that for a small generation rate (corresponding to low light intensity), qV_{oc} can be much smaller than the effective band gap E_{gap}^{eff}. When the incident light intensity is increased, V_{oc} increases logarithmically, but it cannot exceed E_{gap}^{eff}/q, as required by the conservation of energy.

At room temperature, using the values for P, G, and E_{gap}^{eff} given in subsection 2.4.2, we have V_{oc} = 0.85 V, in excellent agreement with the experimental data on MDMO-PPV/PCBM as presented in subsection 2.4.2. This implies that V_{oc} is 0.44 V lower than E_{gap}^{eff}/q, which is due to a voltage loss at the contacts because of band bending.[10] Of course, the magnitude of this loss depends on light intensity and material parameters, as is clear from Eq. (3.11).

Returning to the temperature dependence of V_{oc} , it should be mentioned that the fact that there is no sharply defined band gap strongly complicates the use of Eq. (3.11) to explain temperature dependent measurement of V_{oc} . Due to the presence of energetic disorder in both materials, their HOMO and LUMO levels exhibit a Gaussian broadening of typically 0.1 eV.[13,14] Since the exact distribution of energy levels in the PPV/PCBM blend is not known, the uncertainty in E_{gap}^{eff} is of the same order of magnitude as the variation of V_{oc} with temperature, thereby prohibiting an exact quantitative analysis.

Influence of other types of recombination

The inclusion of another type of non-geminate recombination changes Eq. (3.11) and the light intensity dependence of V_{oc}. One example would be the recombination of free holes with trapped electrons in polymer/polymer solar cells,[15] which is described by Shockley-Read-Hall (SRH) recombination.* Figure 3.7 shows the calculated intensity dependence of V_{oc} when SRH recombination is included, using mobilities and trap densities typical of polymer/polymer solar cells. It follows that the intensity dependence of V_{oc} is much stronger when SRH recombination is included: the slope S increases to 1.66 V_t. The change of slope S when SRH recombination plays a role was also noted for amorphous silicon *p-i-n* junction solar cells.[12] This result suggests that the intensity dependence of V_{oc} may be used as an experimental tool for studying the transport and possible trapping in BHJ solar cells. In this way, Mandoc *el al*. were able to discriminate between trap-free and trap-limited electron transport in polymer/polymer solar cells.[15] In their experiments, S = 1.55 V_t was found, in accordance with SRH recombination. It is important to note that the ideality factor of these devices is even higher (> 2), so the *p-n* junction based model (see section 3.1) cannot explain the experimentally observed intensity dependence.

*One might think of introducing another recombination term in Eq. (3.10) and proceeding with the derivation of an expression for V_{oc}. However, due to the strongly varying density of trapped electrons, the rate constant for SRH recombination will strongly vary throughout the device, and, consequently, the assumption of generation and recombination canceling everywhere breaks down.

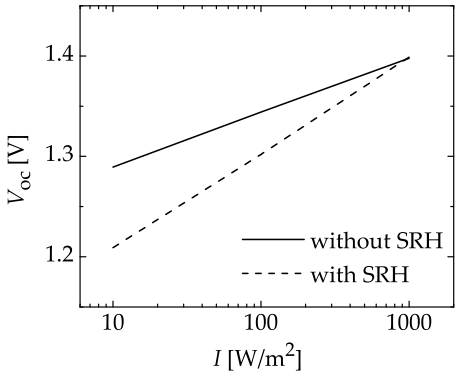

Figure 3.7: Calculated intensity dependence of V_{oc} with and without the inclusion of SRH recombination. When SRH recombination is included, the intensity dependence is much stronger ($S = 1.66\ V_t$).

3.3 Comparison with other solar cells

3.3.1 Influence of non-homogeneity

Up to now, we have only considered BHJs which are homogeneous in their composition. The MIM model predicts that the open-circuit voltage of such BHJs cannot be larger than the difference between the work functions of the electrodes. However, this is not generally true for all types of solar cells. By inducing a concentration gradient of donor and acceptor materials on the molecular scale, a so-called *graded* BHJ can be realized.[16]

Mihailetchi *et al*. have shown that the mobility of electrons and holes in MDMO-PPV/PCBM BHJs depends on the volume ratio of both materials, finding that the mobility through a phase is enhanced when the relative volume of that phase is increased.[17] Additionally, they showed that the highest generation rate of electron-hole pairs G_{max} occurs in a 1:1 (by volume) mixture of MDMO-PPV and PCBM. These results imply that in a graded BHJ both the charge carrier mobilities and the generation rate are highly non-uniform, making it possible to tailor the properties of the active layer in such a way that the zone with the highest charge generation efficiency (i.e., the region with high concentrations of both components) coincides with the maximum of the optical field, while providing efficient carrier transport to the electrodes. The behavior of V_{oc} will be different for such a non-uniform system.*

*In the MDMO-PPV/PCBM system, the dissociation efficiency of bound electron-hole pairs is also strongly dependent on the volume ratio of both components, as discussed in Ref. [17]. As the MDMO-PPV/PCBM system only serves as an illustration, this effect is ignored in the present analysis.

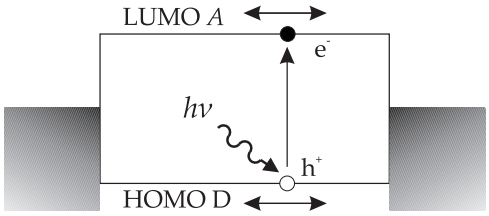

Figure 3.8: A homogeneous BHJ solar cell with electrodes made of the same metal. When no bias voltage is applied, there exists no preferential direction for the charge carriers to go to.

Consider a homogeneous BHJ solar cell with contacts made of the same metal, and assume that the work function is equal to the mean value of the HOMO and LUMO energies, see Fig. 3.8.* In the case of constant (but not necessarily equal) electron and hole mobilities, the short-circuit current would be zero since there is no preferential direction for the charge carriers, consequently, $V_{\rm oc} = 0$. When the profile of the carrier generation rate is strongly asymmetrical, see Fig.. 3.9(a), the open-circuit voltage is still very small.

In the case of electron and hole mobilities which are *not* constant, the predictions by the MIM model are different: Suppose that near the left electrode ($x = 0$), the electron mobility is much higher than near the right electrode ($x = L$), and that the opposite applies to the hole mobility. Now there does exist a preferential direction for the charge carriers, making the carriers flow in opposite directions and hence generating a net (finite) current. It follows that $V_{\rm oc} \neq 0$. Therefore, it is not generally true that the MIM model predicts that the open-circuit voltage is always lower than (or equal to) the difference in work functions of the electrodes. To illustrate this, consider

$$\frac{\mu_n(0)}{\mu_n(L)} = \frac{\mu_p(L)}{\mu_p(0)} = 1000, \tag{3.12}$$

with μ_n exponentially decreasing and μ_p exponentially increasing with x. The calculated current-voltage characteristics for such a device are shown in Fig. 3.9(b). Indeed, the MIM model predicts a finite open-circuit voltage (0.25 V), even in the absence of a difference in work function of the electrodes. Moreover, the results depicted in Fig. 3.9 demonstrate that a nonzero $V_{\rm oc}$ is not so much induced by a non-uniform generation rate, but rather by non-uniform transport properties of the active layer. In principle, this effect may be used advantageously to improve the open-circuit voltage of polymer/fullerene BHJ solar cells with Ohmic contacts.

The most extreme example of a non-homogeneous device structure is a bilayer solar cell.[18] Ramsdale *et al*. demonstrated that the $V_{\rm oc}$ of such a device can indeed be much larger (> 1 V) than the work function difference between the electrodes.[19] This effect

*The exact work function of is of no consequence, the most important requirement, however, is that the work functions of both metals be equal.

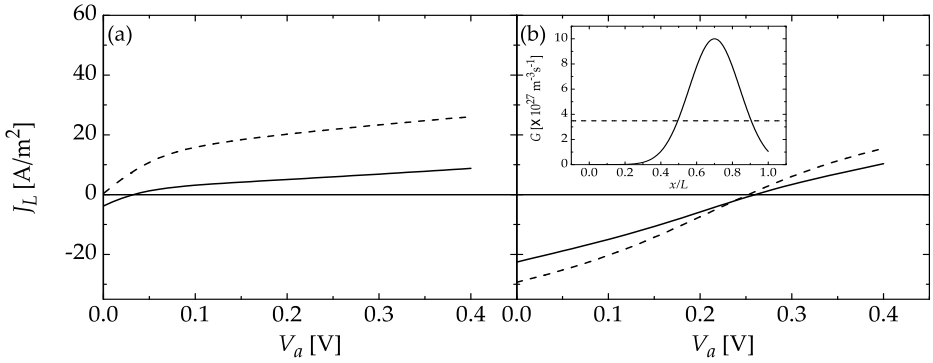

Figure 3.9: (a) Simulated current-voltage characteristics of an illuminated device with equal contacts and constant mobilities. The dashed line corresponds to a constant generation rate G of free charge carriers, while the solid line is calculated by taking the generation profile depicted in part (b) into account. (b) Current-voltage characteristics calculated with mobilities according to Eq. (3.12). The dashed line corresponds to a constant G, while the solid line has been obtained using a generation rate profile as shown in the inset (solid line). The inset also shows the constant generation rate (dashed line) corresponding to average generation rate of the profile.

was attributed to accumulation of charge at the heterojunction giving rise to a diffusion current that must be counterbalanced by a drift current at open-circuit.

3.3.2 Comparison with (in)organic low mobility solar cells

Having discussed the device characteristics of polymer/fullerene BHJ cells it is interesting to compare their operating mechanism with other types of solar cells that also employ low mobility semiconductors as amorphous silicon based *p-i-n* devices.[12,20,21] These devices consist of a thin layer of intrinsic material sandwiched between heavily doped *p* and *n* layers, which function as electrodes. First, the photogeneration of charges in these *p-i-n* devices is fundamentally different: light absorption directly creates free charge carriers since geminate recombination of photogenerated charge carriers is of no importance.[22] In a BHJ device an exciton is created upon light absorption, which subsequently dissociates across the donor/acceptor interface, creating a bound electron-hole pair. This bound pair can either dissociate into free charges contributing to the photocurrent or decay to the ground state, resulting in a strongly field- and temperature-dependent geminate recombination process.[8] This difference is at the heart of our model. Furthermore, bimolecular recombination, and not trapping and subsequent recombination, is the prime loss mechanism of free carriers (i.e., carriers that already escaped the bound electron-hole pair).

The operational principle of dye-sensitized solar cells (DSSCs) has received much attention as well. Such a DSSC consists of a nanoporous titanium dioxide electrode, covered with a monolayer of dye molecules, immersed in a liquid electrolyte containing, e.g., the I^-/I_3^- redox couple.[23] Light is absorbed by the dye layer and consequently, the electrons are transported through the titanium dioxide phase, while the dye molecule is reduced by the I^-/I_3^- redox couple. There has been much debate about whether the driving mechanism of charge transport of these devices is the same as for *p-n* junctions.[24–26] Whereas *p-n* junctions need a built-in field to transport the charges, DSSCs do not seem to need an internal field. Rather, the hole transport through the electrolyte is driven by diffusion, since the electrolyte cannot sustain an electric field. The transport of electrons is less well understood and two models have been proposed:[27] The so-called junction model assumes that electrons are field driven, thereby limiting the open-circuit voltage to the difference in work function of the substrate electrode and the solution redox potential. The kinetic model on the other hand, assumes that the electrons are also driven by diffusion, as are the holes, and that the electric field in the titanium dioxide network is zero due to screening by the electrolyte. Therefore, the charge carriers diffuse away from the interface where they were created, and hence an internal electric field is not needed for photovoltaic action. As a result even a device with equal redox potential and substrate electrode work function can exhibit a nonzero open-circuit voltage. This has indeed been observed for DSSCs,[27] as well as for bilayer devices consisting of conjugated polymers[19] with top and bottom electrodes with the same work function.

It has been asserted that the same should hold for BHJ devices, but that the electric field must also be taken into account since there is no mobile electrolyte to screen the field.[28,29] As a consequence, the open-circuit should not be limited to the difference in electrode work function. However, by varying the work function of the PEDOT:PSS anode, Frohne *et al.* have shown that when the work function of the anode coincides with the LUMO of PCBM, thereby yielding a symmetric device, the open-circuit voltage is zero.[30] Furthermore, Mihailetchi *et al.* also demonstrated, by varying the top electrode (cathode), that the open-circuit voltage is determined by the difference in electrode work function.[10] These results are in full agreement with the metal-insulator-metal picture used here. Since we treat the BHJ as one effective semiconductor, there is no interface for the charge carriers to diffuse away from and the transport is modeled as taking place in only one material, thereby resembling the *p-i-n* junction model. The success of the metal-insulator-metal picture suggests that such diffusion is not important in BHJ solar cells. Not only is this model successful in describing the effect of various electrodes on the open-circuit voltage,[10,30] it also describes, e.g., its light intensity dependence.[31]

3.4 Conclusions

In this chapter, a model for the open-circuit voltage was introduced. By studying the dependency of V_{oc} on incident light intensity, it has been demonstrated that the V_{oc} of BHJ solar cells is inconsistent with *p-n* junction models: Whereas the experimental data

showed that the slope S of V_{oc} as a function of $\ln(I)$ is equal to V_t, the *p-n* junction model predicts a slope of nV_t, where n ranges from 1.35 to 1.98. This phenomenon was observed for two different PPV derivatives as donor material. The main cause of this discrepancy lies in the fact that the strong voltage dependence of the photogenerated current is not taken into account.

An alternative model for the open-circuit voltage has been presented, based on the notion that the quasi-Fermi potentials are constant throughout the device. Subsequently, a formula for V_{oc} was derived, consistently explaining the light intensity dependence of the open-circuit voltage of polymer/fullerene bulk heterojunction devices with Ohmic contacts. Next, the predictions of the MIM model and its relation to other types of solar cells have been discussed.

References

[1] C. J. Brabec, A. Cravino, D. Meissner, N. S. Sariciftci, T. Fromherz, M. T. Rispens, L. Sanchez, and J. C. Hummelen, Adv. Funct. Mater. **11**, 374 (2001).

[2] V. D. Mihailetchi, P. W. M. Blom, J. C. Hummelen, and M. T. Rispens, J. Appl. Phys. **94**, 6849 (2003).

[3] S. M. Sze, *Physics of semiconductor devices* (Wiley, New York, 1981).

[4] E. A. Katz, D. Faiman, S. M. Tuladhar, J. M. Kroon, M. M. Wienk, T. Fromherz, F. Padinger, C. J. Brabec, and N. S. Sariciftci, J. Appl. Phys. **90**, 5343 (2001).

[5] D. Chirvase, Z. Chiguvare, M. Knipper, J. Parisi, V. Dyakonov, and J. C. Hummelen, J. Appl. Phys. **93**, 3376 (2003).

[6] P. Schilinsky, C. Waldauf, and C. J. Brabec, Appl. Phys. Lett. **81**, 3885 (2002).

[7] I. Riedel, J. Parisi, V. Dyakonov, L. Lutsen, D. Vanderzande, and J. C. Hummelen, Adv. Funct. Mater. **14**(1), 38 (2004).

[8] V. D. Mihailetchi, L. J. A. Koster, J. C. Hummelen, and P. W. M. Blom, Phys. Rev. Lett. **93**, 216601 (2004).

[9] P. Schilinsky, C. Waldauf, J. Hauch, and C. J. Brabec, J. Appl. Phys. **95**, 2816 (2004).

[10] V. D. Mihailetchi, P. W. M. Blom, J. C. Hummelen, and M. T. Rispens, J. Appl. Phys. **94**, 6849 (2003).

[11] S. Selberherr, *Analysis and Simulation of Semiconductor Devices* (Springer-Verlag, Wien, 1984).

[12] E. A. Schiff, Sol. Energy Mater. Sol. Cells **78**, 567 (2003).

[13] H. Bässler, Phys. Status Solidi B **175**, 15 (1993).

[14] V. D. Mihailetchi, J. K. J. van Duren, P. W. M. Blom, J. C. Hummelen, R. A. J. Janssen, J. M. Kroon, M. T. Rispens, W. J. H. Verhees, and M. M. Wienk, Adv. Funct. Mater. **13**, 43 (2003).

[15] M. M. Mandoc, W. Veurman, L. J. A. Koster, M. M. Koeste, J. Sweelssen, B. de Boer, and P. W. M. Blom (unpublished).

[16] B. Pradhan and A. J. Pal, Synth. Met. **155**, 555 (2005).

[17] V. D. Mihailetchi, L. J. A. Koster, P. W. M. Blom, C. Melzer, B. de Boer, J. K. J. van Duren, and R. A. J. Janssen, Adv. Funct. Mater. **15**, 795 (2005).

[18] C. W. Tang, Appl. Phys. Lett. **48**, 183 (1986).

[19] C. M. Ramsdale, J. A. Barker, A. C. Arias, J. D. MacKenzie, R. H. Friend, and N. C. Greenham, J. Appl. Phys. **92**, 4266 (2002).

[20] P. Chatterjee, J. Appl. Phys. **76**, 1301 (1994).

[21] F. A. Rubinelli, R. Jiménez, J. K. Rath, and R. E. I. Schropp, J. Appl. Phys. **91**, 2409 (2002).

[22] F. Carasco and W. E. Spear, Philos. Mag. B **47**, 495 (1983).

[23] M. Grätzel, Prog. Photovolt. Res. Appl. **8**, 171 (2000).

[24] K. Schwarzburg and F. Willig, J. Phys. Chem. B **107**, 3552 (2003).

[25] G. Kron, T. Egerter, J. H. Werner, and U. Rau, J. Phys. Chem. B **107**, 3556 (2003).

[26] B. A. Gregg, J. Phys. Chem. B **107**, 13540 (2003); J. Bisquert, *ibid*. **107**, 13541 (2003); J. Augustynski, *ibid*. **107**, 13544 (2003); K. Schwarzburg and F. Willig, *ibid*. **107**, 13546 (2003); U. Rau, G. Kron, and J. H. Werner, *ibid*. **107**, 13547 (2003).

[27] F. Pichot and B. A. Gregg, J. Phys. Chem. B **104**, 6 (2000).

[28] B. A. Gregg and M. C. Hanna, J. Appl. Phys. **93**, 3605 (2003).

[29] B. A. Gregg, J. Phys. Chem. B **107**, 4688 (2003).

[30] H. Frohne, S. E. Shaheen, C. J. Brabec, D. C. Müller, N. S. Sariciftci, and K. Meerholz, ChemPhysChem **9**, 795 (2002).

[31] L. J. A. Koster, V. D. Mihailetchi, R. Ramaker, and P. W. M. Blom, Appl. Phys. Lett. **86**, 123509 (2005).